High-Density Ultracold Neutron Source for Low-Energy Particle Physics Experiments

Skyler Degenkolb, ^{1, 2, *} Estelle Chanel, ^{2, †} Simon Baudoin, ² Marie-Hélène Baurand, ² Douglas H. Beck, ³ Juliette Blé, ² Eric Bourgeat-Lami, ² Zeus Castillo, ² Hanno Filter, ² Maurits van der Grinten, ⁴ Tobias Jenke, ² Michael Jentschel, ² Victorien Joyet, ² Eddy Lelièvre-Berna, ² Husain Manasawala, ¹ Thomas Neulinger, ^{5, 2} Peter Fierlinger, ⁶ Kseniia Svirina, ^{2, 1} Xavier Tonon, ² and Oliver Zimmer ²

¹ Physikalisches Institut, Universität Heidelberg, Im Neuenheimer Feld 226, 69120 Heidelberg, Germany

² Institut Laue-Langevin, CS 20156, 38042 Grenoble Cedex 9, France

³ Department of Physics, University of Illinois at Urbana-Champaign,

1110 West Green Street, Urbana, IL 61801 USA

⁴ Particle Physics Department, STFC Rutherford Appleton Laboratory, UK

⁵ FRM II, Lichtenbergstraße 1, 85748 Garching bei München, Germany

⁶ Physikdepartment, Technische Universität München,

James-Franck-Straße 1, 85748 Garching bei München, Germany

(Dated: April 18, 2025)

SuperSUN, a new superthermal source of ultracold neutrons (UCN) at the Institut Laue-Langevin, exploits inelastic scattering of neutrons in isotopically pure superfluid ⁴He at temperatures below 0.6 K. For the first time, continuous operation with an intense broad-spectrum cold neutron beam is demonstrated over 60 days. We observe continuous UCN extraction rates of 21000 s⁻¹, and storage in the source with saturated *in-situ* density 273 cm⁻³. The high stored density, low-energy UCN spectrum, and long storage times open new possibilities in fundamental and applied physics.

Introduction—Ultracold neutrons (UCN) provide a route to high-precision experiments via long holding times [1-3]. Precision measurements and searches for new physics are thus possible with relatively small numbers of stored UCN, including measurements of the neutron's permanent electric dipole moment (EDM) [4] and lifetime [5], angular correlations in β decay [6], bound states in Earth's gravity [7, 8], tests of Lorentz invariance [9, 10], searches for axion-like new particles [11], and limits on the oscillation of neutrons to other neutral particles [12]. Nevertheless, low statistics has been a longstanding challenge for fundamental UCN science and a major obstacle to applications. We present the first full implementation of a nearly 50-year-old concept to resolve this challenge [13], following many proof-ofprinciple demonstrations [14–22].

We distinguish two categories of UCN source: "flux sources" delivering a high particle current, and "density sources" characterized by high numbers of stored neutrons per unit volume. High densities are achieved by equilibrating high UCN production rate densities against low total loss rates. Since production and loss are energy-dependent, the energy spectrum of stored UCN at saturated equilibrium can vary greatly between sources and different operating conditions. This also impacts UCN storage and transfer [23]: because low-energy UCN are less affected by important loss channels, long time constants are characteristic of soft UCN spectra. Technical details such as material choices and mechanical tolerances strongly impact UCN loss.

Superfluid helium is the only production medium within which UCN loss can, in principle, be arbitrarily reduced to approach the natural limit imposed by β decay. The dominant UCN production channel is

"conversion" of a cold neutron with 0.89 nm wavelength, which transfers nearly its entire energy and momentum to the superfluid by creating a single phonon. The known UCN production cross-section and wavelength dependence [17, 24] result in an approximately isotropic distribution of wavevectors \mathbf{k} [25], and a differential energy spectrum scaling as $\sqrt{E}dE \propto |\mathbf{k}|^2 d|\mathbf{k}|$ [13]. Absorption losses are entirely absent in ⁴He, while ³He is a strong neutron absorber. Up-scattering out of the UCN energy range is negligible at temperatures $T \lesssim 0.6 \,\mathrm{K}$ [26].

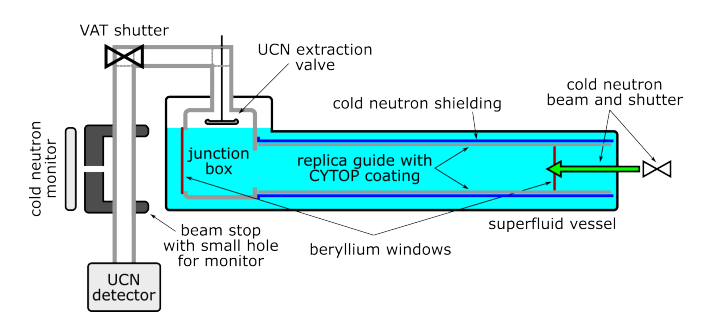


FIG. 1. Diagram of SuperSUN, indicating the main neutron-handling elements. A 90° bend in the horizontal extraction guide, before the VAT shutter and out of the plane of the page, displaces the vertical guide leading to the detector out of the path of the cold neutron beam.

We report initial measurements of superthermal UCN production from the SuperSUN source at the Institut Laue-Langevin (ILL) in Grenoble [27]. After briefly describing the apparatus, we characterize UCN buildup within the source, loss of UCN during holding (in-situ storage), and performance in the continuous "open converter" extraction mode. Total UCN production at saturation is 4.5 times that of a prototype source at the ILL

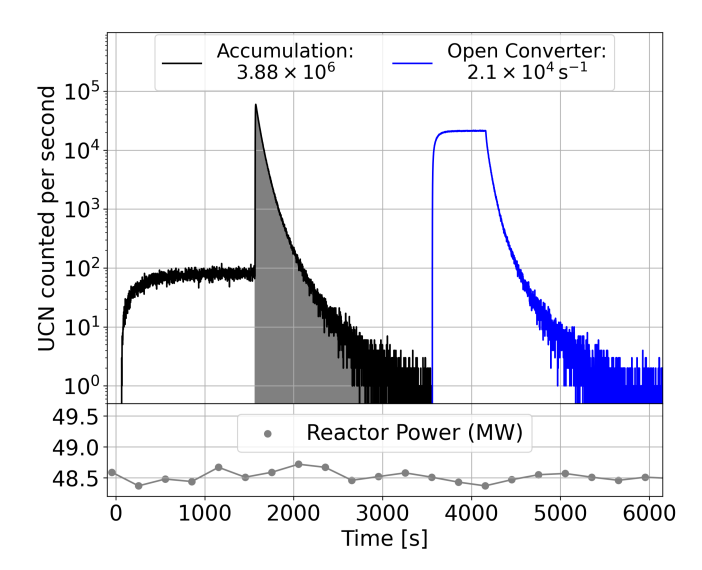


FIG. 2. Example data for two operating modes. Left (black data series): UCN accumulate for 1500 s in the closed converter, after which the cold neutron beam is shut off and the UCN extraction valve opens. The total number of extracted UCN equals the shaded area under the peak: 3.88×10^6 . Right (blue data series): a lower, but steady, rate of 2.1×10^4 s⁻¹ is continuously extracted from the converter by fixing the UCN extraction valve open during beam delivery. After a chosen interval (600 s) the beam is shut off.

[28, 29], exceeding earlier demonstrations by a factor 14 [19, 21] and achieving the largest UCN density stored and measured to date.

Apparatus—Figure 1 shows a diagram of SuperSUN. The cold neutron beamline H523 originates in a liquid deuterium moderator, and terminates at the UCN source [29]. Gammas and short-wavelength neutrons are suppressed by a strongly curved guide made of m = 1.2supermirrors [30]. A final guide section with m = 2.5and a tapered octagonal cross section [31] adapts the rectangular guide to the circular cross-section of Super-SUN's converter, which is transversely bounded by a 3 m long replica-type guide [32, 33] of 74.4 mm inner diameter. The replica guide consists of a laser-cut, rolled, and laser-welded Ni foil $\sim 150 \,\mu\mathrm{m}$ thick, with a m=3 supermirror coating on its inner surface consisting of about 600 layers. Cold neutrons enter the converter through a 1 mm thick beryllium window, at which position the differential flux at $0.89 \,\mathrm{nm}$ is $2.7 \times 10^9 \,\mathrm{cm}^{-2} \,\mathrm{s}^{-1} \,\mathrm{nm}^{-1}$. Guiding increases the mean cold neutron path length in helium nearly an order of magnitude, to maximize UCN production at high density. Neutrons escaping through the replica foil are absorbed in 0.2 mm of metallic Gd before reaching the wall of the surrounding superfluid vessel. The converter volume is filled with superfluid ⁴He via a packed-alumina superleak [34, 35], reducing ³He contamination. To reduce UCN loss the cylindrical guide wall is coated with the fluoropolymer CYTOP [36], with neutron optical potential 115 neV and loss factor

 $\eta \leq (2.7 \pm 0.2) \times 10^{-5}$ at 10 K [37]. A beryllium-coated aluminum junction box couples this guide to a vertical extraction system. A second beryllium window, through which cold neutrons exit the converter, closes its downstream side. The circular extraction aperture is sealed during UCN accumulation and storage by a diamondlike carbon (DLC) coated aluminum disk. A linear actuator lowers this disk valve to release stored UCN for experiments, the free superfluid helium surface remaining below its range of motion. UCN leaving the helium can exit the converter through 50 mm diameter polished stainless steel guides, passing two 90° bends that incorporate Ge windows coated with deuterium-enriched DLC [38]. These windows reflect UCN while transmitting infrared thermal radiation out of the extraction guide, lowering the heat load on the converter. To reduce UCN loss, mechanical gaps are minimized, nominally 0.1 mm or less for all neutron-optical components.

A recirculating ³He evaporation refrigerator absorbs heat delivered to the converter via mechanical supports, thermal radiation, and absorption of cold neutrons. SuperSUN operates at 0.56 K with the beam shut off. The cold neutron beam adds 20-25 mW heating for nominal beam flux, increasing the converter temperature by about 30 mK and the (still negligible) loss rate of UCN via upscattering by 40%. Thermal screens and internal liquid helium reservoirs are cooled by three cryocoolers (Sumitomo RDK-415D). Liquid helium is filled from a dewar into a 100-liter internal reservoir, and cooled to superfluid by pumping a separate "1 K pot". A finned heat exchanger at the bottom of the ³He pumping column is used to cool purified ⁴He at the point where it arrives in the converter. SuperSUN is brought into operation within 8 days and operates continuously for full reactor cycles, typically 7-9 weeks, with the liquid helium reservoir refilled weekly.

Characterization—We establish accumulation and storage properties of the converter, and UCN production rates for two different operation modes: accumulation and open converter. Data illustrating these modes are shown in Fig. 2. After a 60 s background measurement (background rates are in fact negligible), the cold neutron beam was opened and UCN accumulated in the converter for 1500 s with the extraction valve closed. The detected leakage rate approached $80 \,\mathrm{s}^{-1}$ at saturation, due to a small monitoring hole drilled in the valve disk. The beam was then shut off, and the extraction valve opened after a 1s holding delay. UCN then exited the source, gaining 18.5 neV by leaving the helium, and rising 28.5 cm from the midline of the converter to the midline of the horizontal extraction guide [39]. After exiting the source UCN fell 82 cm in a vertical guide, exceeding the normal momentum needed to enter a DUNya-type ³He-based UCN detector [40] through a 100 μ m aluminum window. The total number of UCN detected in the 2000 s counting interval was 3.88×10^6 without any corrections, within 5%

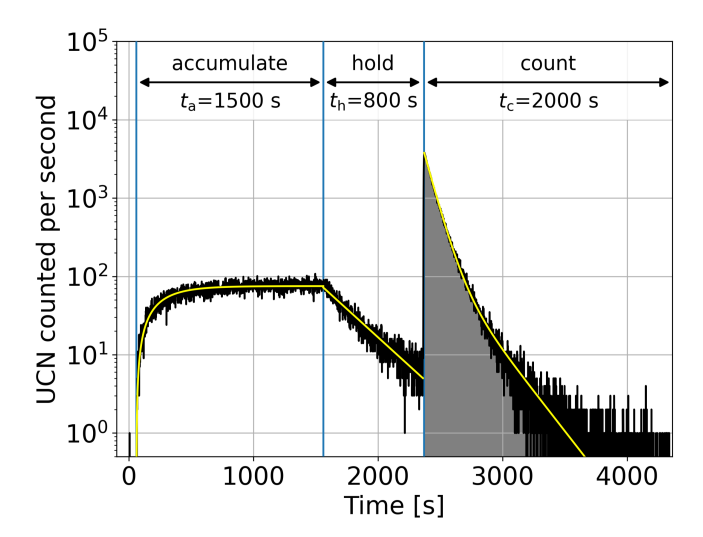


FIG. 3. Detected UCN rate during an accumulation-mode measurement with delayed extraction (i.e., storage without UCN production). The background and accumulation intervals are as in Fig. 2, followed by an 800 s holding period with the cold neutron beam shut off and the extraction valve closed. UCN are then extracted and counted for 2000 s. The fit functions are defined in Eqs. (1)-(3).

of the design goal [28].

Open converter measurements can be understood as a limiting case where UCN are produced continuously, and loss from the converter is dominated by the steady extraction rate. The detected continuous rate of $2.1 \times 10^4 \ \mathrm{s}^{-1}$ thus equilibrates the (constant) total production rate in the converter against the depletion resulting from UCN escaping.

Around 1575 s in Fig. 2 the peak event rate 6.3×10^4 s⁻¹ includes pileup, where a single detection event represents

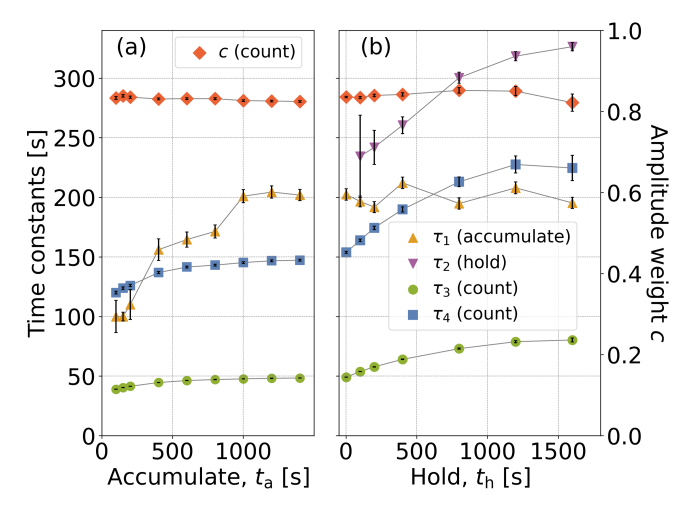


FIG. 4. Variation of fit parameters (a) with accumulation time for fixed $t_{\rm h}=0$ s, and (b) with holding time for fixed $t_{\rm a}=1500$ s. The fit functions are defined in Eqs. (1)-(3), and error bars are from unbinned fits.

more than one neutron. We apply pileup corrections, up to event multiplicity four and totaling less than 10% for the highest rates, to obtain time constants for accumulation and storage, i.e., for fits to data and throughout Figs. 3-5. Corrections are not applied to our values for total UCN output or density, which are therefore conservative. The converter's 14.2-liter volume gives the saturated UCN density in-situ as 273 cm⁻³. To our knowledge this is the highest stored UCN density of any measurement to date.

Storage properties of the converter were studied by independently varying the accumulation and holding intervals, respectively t_a and t_h . The UCN extraction valve was open only during the counting periods, of duration $t_c = 2000$ s, and the cold neutron beam was present only during accumulation. As shown in Fig. 3 for one example, each phase of the measurement displays a characteristic trend of the detected UCN rate. In each phase, unbinned data are fit to a probability density model using maximum-likelihood estimation (MLE). The fit lines for binned data shown in Fig. 3 are obtained by scaling the MLE probability densities by the factor $N\Delta t$, where N is the total number of events in that phase and Δt is the bin width. Fits are performed setting t=0 at the beginning of each measurement phase. We emphasize that these models are essentially phenomenological: strictly speaking, in each spectrum there is a distinct time constant for each UCN energy.

A saturation model with one time constant is used for the accumulation phase,

$$f_{\mathbf{a}}(t;\tau_1) = \frac{1 - e^{-t/\tau_1}}{t_{\mathbf{a}} - \tau_1(1 - e^{-t_{\mathbf{a}}/\tau_1})},\tag{1}$$

where the denominator ensures $\int_0^{t_a} f_a(t)dt = 1$ and t_a is the duration of accumulation as shown in Fig. 3. For the holding phase a normalized single-exponential is used,

$$f_{\rm h}(t;\tau_2) = \frac{e^{-t/\tau_2}}{\tau_2 \left(1 - e^{-t_{\rm h}/\tau_2}\right)}.$$
 (2)

A sum of two exponentials is used for the counting phase:

$$f_{c}(t; c, \tau_{3}, \tau_{4}) = c \frac{e^{-t/\tau_{3}}}{\tau_{3}} + (1 - c) \frac{e^{-t/\tau_{4}}}{\tau_{4}}.$$
 (3)

Fit parameters follow the semicolons.

Figure 4 shows the impact of varying accumulation or holding time, by plotting the fit parameters for each phase (connecting lines are guides for the eye). The UCN spectrum evolves during all measurement phases, due to energy dependence of losses. We therefore do not expect identical ensemble-averaged time constants for accumulation and storage, although the same loss mechanisms determine both. A trend towards longer time constants with increasing $t_{\rm a}$ or $t_{\rm h}$ also ensues, as the time-averaged UCN loss probability increases monotonically with energy. The in-situ spectrum therefore becomes softer over

time, leading to both lower ensemble-averaged loss rates and slower extraction to the detector. Note that due to fixing $t_{\rm a}$, variation of $\tau_{\rm 1}$ is not expected in Fig. 4(b).

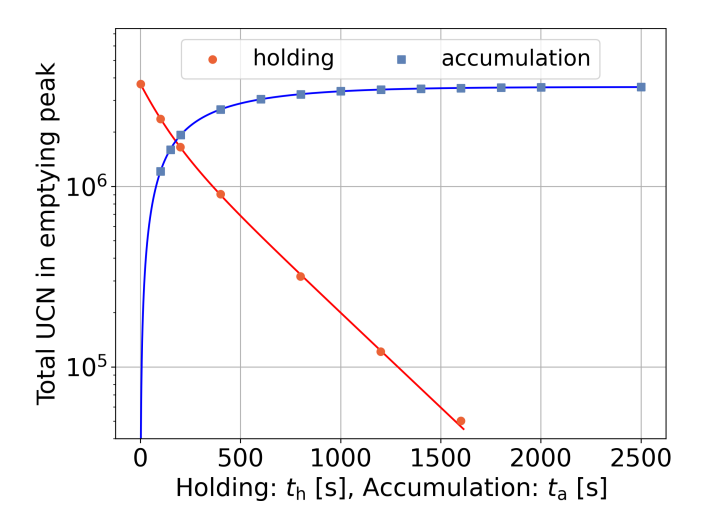


FIG. 5. Variation of the total extracted UCN number with the duration of holding (red, $t_a = 1500 \,\mathrm{s}$) or accumulation (blue, $t_h = 0 \,\mathrm{s}$) in the source. Error bars are smaller than the data markers. Equations (4)-(5) give the fit functions.

It is instructive to plot total extracted UCN as a function of the holding or accumulation time, on a common abscissa, as done in Fig. 5. For both cases the ordinate represents an integral of the entire counting peak. To compensate possible drifts of the cold neutron beam intensity, each data point is scaled by the ratio of average beam intensity during the accumulation phase to the average beam intensity across the entire data series. This is a correction of at most a few percent, and typically much less.

Equations (1) and (3) are adapted for fitting the discrete data of Fig. 5. Representing each data point as (t_i, N_i) , the bi-exponential fit function for holding is:

$$g_{c}(t; c, \tau_{3}, \tau_{4}) = \frac{f_{c}(t; c, \tau_{3}, \tau_{4}) \sum_{i} N_{i}}{\sum_{i} f_{c}(t_{i}; c, \tau_{3}, \tau_{4})}.$$
 (4)

The higher-statistics data of the accumulation series now require in addition a second time constant that we denote τ'_1 :

$$g_{\mathbf{a}}(t; a, \tau_1, \tau_1') = \frac{[af_{\mathbf{a}}(t; \tau_1) + (1-a)f_{\mathbf{a}}(t; \tau_1')] \sum_i N_i}{\sum_i [af_{\mathbf{a}}(t_i; \tau_1) + (1-a)f_{\mathbf{a}}(t_i; \tau_1')]}.$$
(5)

Here a is a weight parameter, analogous to c in Eqs. (3) and (4). Overall normalization in Eqs. (4) and (5) is fixed by the data. The fit results for storage are $c = 0.17 \pm 0.02$, $\tau_3 = 117 \, \text{s} \pm 10 \, \text{s}$, and $\tau_4 = 414 \, \text{s} \pm 9 \, \text{s}$. For accumulation, we obtain $a = 0.42 \pm 0.03$, $\tau_1 = 131 \, \text{s} \pm 7 \, \text{s}$, and $\tau_1' = 410 \, \text{s} \pm 13 \, \text{s}$.

Storage data later in the same reactor cycle gave $c=0.20\pm0.03,\, \tau_3=152\,\mathrm{s}\pm11\,\mathrm{s},\, \mathrm{and}\,\, \tau_4=427\,\mathrm{s}\pm10\,\mathrm{s}.$

Given that the converter was warmed to 1 K between these measurement series, changing internal conditions such as the superfluid level or concentration of ³He may be responsible for longer time constants. It is not possible, on the basis of these phenomenological fit functions, to distinguish underlying mechanisms.

Our measurements were intentionally performed without a separation foil, and interspersed with repeated monitoring measurements. These show compounding losses of $\sim 3\%$ per day in total UCN output. Based on demonstrations already performed at the SUN-2 prototype source [28, 29], a $0.5\,\mu\mathrm{m}$ polypropylene foil is expected to reduce degradation to negligible levels at the expense of 10% (static) reduction in total UCN output.

Discussion—UCN produced in ⁴He have very low energies [41], and high phase-space density. Apart from SuperSUN, all full-scale UCN sources to date are flux sources, with harder UCN spectra [42-44] and more dilute phase space. Soft spectra are highly advantageous in storage experiments, complementing shorter and flowthrough type measurements at flux sources. Extracting UCN enables external storage experiments, with significant gains overcoming polarization and transport losses. This approach is most advanced for a neutron EDM measurement at SuperSUN (PanEDM), where 250 s measurement duration and a 400 s repetition period enable reaching 75% of the saturated maximum between fills. Sensitivities projected from this performance can be globally leading [28], and other storage experiments should profit similarly.

For *in-situ* storage the full phase-space density of the source is usable, achieving high statistics not presently available from any other UCN source or production technology. We open the door to *in-situ* measurements with further gains of an order-of-magnitude or more [45–47], and novel possibilities such as storage of gravitationally bound states for fundamental physics and applications.

Summary and outlook—We have reported first UCN production from the new SuperSUN source at the ILL. The effective time constants for accumulation are 131 s and 410 s, while bi-exponential fits give 107-163 s and 405-437 s for in-situ UCN storage. Variation of fit parameters with accumulation or storage intervals is consistent with expected evolution of the UCN spectrum. The maximum number of UCN stored to date in-situ was 3.88×10^6 , giving an uncorrected density of 273 cm⁻³. This is the highest ever measured, and enables qualitatively and quantitatively new measurements with UCN.

The first use of the source will be supplying UCN to the PanEDM neutron electric dipole moment experiment. A second phase for SuperSUN will incorporate a superconducting octupole magnet, to generate a radial magnetic gradient with the field reaching 2.1 T at the boundary surface of the converter. This gives a deeper trap for low-field seeking UCN, and increased loss for high-field seekers [48]. Polarized UCN will therefore accumulate in

the converter, and the extraction system and transport guides will be modified to preserve UCN polarization.

Acknowledgements—This project was funded by the Agence Nationale de la Recherche (ANR) under the grant ANR-14-CE33-0023-01, and by the Institut Laue—Langevin's Endurance program. We would also like to thank Ulrich Schmidt, Felix Waldherr, and Lukas Dimmler for support and discussions, as well as the entire PanEDM collaboration, and technical services of the ILL, TUM, and Heidelberg University. We also gratefully acknowledge S-DH GmbH, for extensive joint work developing novel cold neutron guides for SuperSUN.

- * Contact author: degenkolb@physi.uni-heidelberg.de † Contact author: chanele@ill.fr
- [1] A. Steyerl, Ultracold Neutrons (World Scientific, 2020).
- [2] R. Golub, D. Richardson, and S. Lamoreaux, *Ultra-Cold Neutrons* (CRC Press, 1991).
- [3] V. K. Ignatovich, The physics of ultracold neutrons (Clarendon Press, 1990).
- [4] C. Abel, S. Afach, N. J. Ayres, C. A. Baker, G. Ban, G. Bison, K. Bodek, V. Bondar, M. Burghoff, E. Chanel, et al., Measurement of the permanent electric dipole moment of the neutron, Phys. Rev. Lett. 124, 081803 (2020).
- [5] F. M. Gonzalez, E. M. Fries, C. Cude-Woods, T. Bailey, M. Blatnik, L. J. Broussard, N. B. Callahan, J. H. Choi, S. M. Clayton, S. A. Currie, et al. (UCN τ Collaboration), Improved neutron lifetime measurement with UCN τ , Phys. Rev. Lett. **127**, 162501 (2021).
- [6] M. P. Mendenhall, R. W. Pattie, Y. Bagdasarova, D. B. Berguno, L. J. Broussard, R. Carr, S. Currie, X. Ding, B. W. Filippone, A. García, et al. (UCNA Collaboration), Precision measurement of the neutron β-decay asymmetry, Phys. Rev. C 87, 032501 (2013).
- [7] G. Cronenberg, P. Brax, H. Filter, P. Geltenbort, T. Jenke, G. Pignol, M. Pitschmann, M. Thalhammer, and H. Abele, Acoustic Rabi oscillations between gravitational quantum states and impact on symmetron dark energy, Nature Phys. 14, 1022 (2018).
- [8] T. Jenke, J. Bosina, J. Micko, M. Pitschmann, R. Sedmik, and H. Abele, Gravity resonance spectroscopy and dark energy symmetron fields: qBOUNCE experiments performed with Rabi and Ramsey spectroscopy, Eur. Phys. J. ST 230, 1131 (2021), arXiv:2012.07472 [hep-ph].
- [9] I. Altarev, C. A. Baker, G. Ban, G. Bison, K. Bodek, M. Daum, P. Fierlinger, P. Geltenbort, K. Green, M. G. D. van der Grinten, et al., Test of Lorentz invariance with spin precession of ultracold neutrons, Phys. Rev. Lett. 103, 081602 (2009).
- [10] A. N. Ivanov, M. Wellenzohn, and H. Abele (qBounce), Tests of Lorentz-Invariance Violation in the Standard-Model Extension with Ultracold Neutrons in qBounce Experiments, in 8th Meeting on CPT and Lorentz Symmetry (2020) pp. 118–121.
- [11] N. J. Ayres, G. Bison, K. Bodek, V. Bondar, T. Bouil-laud, E. Chanel, P.-J. Chiu, B. Clement, C. B. Crawford, M. Daum, et al., Search for an interaction mediated by axion-like particles with ultracold neutrons at the PSI,

- New J. Phys. 25, 103012 (2023).
- [12] G. Ban, J. Chen, T. Lefort, O. Naviliat-Cuncic, W. Saenz-Arevalo, P.-J. Chiu, B. Clément, P. Larue, G. Pignol, S. Roccia, M. Guigue, T. Jenke, B. Perriolat, and P. Schmidt-Wellenburg, Search for neutron-tohidden-neutron oscillations in an ultracold neutron beam, Phys. Rev. Lett. 131, 191801 (2023).
- [13] R. Golub and J. Pendlebury, The interaction of ultra-cold neutrons (UCN) with liquid helium and a superthermal UCN source, Physics Letters A 62, 337 (1977).
- [14] P. Ageron, W. Mampe, R. Golub, and J. Pendelbury, Measurement of the ultra cold neutron production rate in an external liquid helium source, Physics Letters A 66, 469 (1978).
- [15] R. Golub, C. Jewell, P. Ageron, W. Mampe, B. Heckel, and I. Kilvington, Operation of a superthermal ultra-cold neutron source and the storage of ultra-cold neutrons in superfluid helium 4, Zeitschrift für Physik B Condensed Matter 51, 187 (1983).
- [16] C. R. Brome et al., Magnetic trapping of ultracold neutrons, Phys. Rev. C 63, 055502 (2001), arXiv:nuclex/0103003.
- [17] C. Baker, S. Balashov, J. Butterworth, P. Geltenbort, K. Green, P. Harris, M. van der Grinten, P. Iaydjiev, S. Ivanov, J. Pendlebury, D. Shiers, M. Tucker, and H. Yoshiki, Experimental measurement of ultracold neutron production in superfluid ⁴He, Physics Letters A 308, 67 (2003).
- [18] O. Zimmer, K. Baumann, M. Fertl, B. Franke, S. Mironov, C. Plonka, D. Rich, P. Schmidt-Wellenburg, H. F. Wirth, and B. van den Brandt, A Superfluid helium converter for accumulation and extraction of ultracold neutrons, Phys. Rev. Lett. 99, 104801 (2007), arXiv:0705.3960 [nucl-ex].
- [19] O. Zimmer, F. M. Piegsa, and S. N. Ivanov, Superthermal source of ultracold neutrons for fundamental physics experiments, Phys. Rev. Lett. 107, 134801 (2011).
- [20] Y. Masuda, K. Hatanaka, S.-C. Jeong, S. Kawasaki, R. Matsumiya, K. Matsuta, M. Mihara, and Y. Watanabe, Spallation Ultracold Neutron Source of Superfluid Helium below 1 K, Phys. Rev. Lett. 108, 134801 (2012).
- [21] F. M. Piegsa, M. Fertl, S. N. Ivanov, M. Kreuz, K. K. H. Leung, P. Schmidt-Wellenburg, T. Soldner, and O. Zimmer, New source for ultracold neutrons at the Institut Laue-Langevin, Phys. Rev. C 90, 015501 (2014), arXiv:1404.3527 [physics.ins-det].
- [22] S. Ahmed, E. Altiere, T. Andalib, B. Bell, C. P. Bidinosti, E. Cudmore, M. Das, C. A. Davis, B. Franke, M. Gericke, et al. (TUCAN), First ultracold neutrons produced at TRIUMF, Phys. Rev. C 99, 025503 (2019).
- [23] G. Bison, M. Daum, K. Kirch, B. Lauss, D. Ries, P. Schmidt-Wellenburg, G. Zsigmond, T. Brenner, P. Geltenbort, T. Jenke, et al., Comparison of ultracold neutron sources for fundamental physics measurements, Phys. Rev. C 95, 045503 (2017).
- [24] P. Schmidt-Wellenburg, K. Andersen, and O. Zimmer, Ultra cold neutron production by multiphonon processes in superfluid helium under pressure, Nuclear Instruments and Methods in Physics Research Section A: Accelerators, Spectrometers, Detectors and Associated Equipment 611, 259 (2009), Particle Physics with Slow Neutrons.
- [25] S. K. Lamoreaux and R. Golub, Angular distribution of ultracold neutrons produced by scattering of cold neu-

- trons in superfluid ⁴He, Sov. Phys. JETP Lett. **58**, 792 (1993).
- [26] R. Golub, On the storage of neutrons in superfluid ⁴He, Physics Letters A 72, 387 (1979).
- [27] E. Chanel, D. Beck, J. Blé, S. Degenkolb, C. Desalme, L. Dimmler, R. Georgii, M. H.M., T. Neulinger, and F. Waldherr, Characterization of SuperSUN phase I, part I, Institut Laue-Langevin (ILL) doi:10.5291/ILL-DATA.TEST-3284 (2023).
- [28] D. Wurm, D. H. Beck, T. Chupp, S. Degenkolb, K. Fierlinger, P. Fierlinger, H. Filter, S. Ivanov, C. Klau, M. Kreuz, et al., The PanEDM neutron electric dipole moment experiment at the ILL, EPJ Web Conf. 219, 02006 (2019).
- [29] E. Chanel, S. Baudoin, M.-H. Baurand, N. Belkhier, E. Bourgeat-Lami, S. Degenkolb, M. van der Grinten, M. Jentschel, V. Joyet, M. Kreuz, et al., Concept and strategy of SuperSUN: A new ultracold neutron converter, Journal of Neutron Research 24, 111 (2022).
- [30] The "m-value" of multilayer coatings used for neutron supermirrors is the factor by which the critical angle exceeds that of Ni with natural isotopic composition.
- [31] S. Degenkolb, M. Kreuz, and O. Zimmer, A tapered transition guide with irregular octagonal cross-section, Journal of Neutron Research 20, 117 (2018).
- [32] C. Plonka, P. Geltenbort, T. Soldner, and H. Häse, Replika mirrors—nearly loss-free guides for ultracold neutrons—measurement technique and first preliminary results, Nuclear Instruments and Methods in Physics Research Section A: Accelerators, Spectrometers, Detectors and Associated Equipment 578, 450 (2007).
- [33] A. P. Serebrov, A. Vasil'ev, M. S. Lasakov, E. Siber, A. N. Murashkin, A. I. Egorov, A. K. Fomin, S. V. Sbitnev, P. Geltenbort, and O. Zimmer, Replica neutron guides for experiments with ultracold neutrons, Technical Physics 62, 164 (2017).
- [34] O. Zimmer, P. Schmidt-Wellenburg, M. Fertl, H. F. Wirth, M. Assmann, J. Klenke, and B. van den Brandt, Ultracold neutrons extracted from a superfluid-helium converter coated with fluorinated grease, Eur. Phys. J. C 67, 589 (2010).
- [35] H. Yoshiki, H. Nakai, and E. Gutsmiedl, A new superleak to remove He³ for UCN experiments, Cryogenics 45, 399 (2005).
- [36] A. G. C. Chemicals Inc., Amorphous Fluoropolymer CYTOP, https://www.agc-chemicals.com/file.jsp? id=jp/en/fluorine/products/cytop/download/pdf/ CYTOP_EN_Brochure.pdf, accessed: 2024-03-12.
- [37] T. Neulinger, D. Beck, E. Connolly, S. Degenkolb, P. Fierlinger, H. Filter, J. Hingerl, P. Nordin, T. Saerbeck, and O. Zimmer, Ultracold neutron storage in a bot-

- tle coated with the fluoropolymer CYTOP, Eur. Phys. J. A 58, 141 (2022).
- [38] Hydrogen impurities in DLC can significantly reduce its neutron optical potential. These DLC coatings are prepared with deuterated precursor chemicals, to maintain a high scattering length density despite impurities.
- [39] The minimum total UCN energy for extraction is \sim 15 neV higher than the lowest total UCN energy that can exist in the source, implying that approximately 5% of the UCN produced are unable to exit the source.
- [40] L. Groshev, V. Dvoretskij, A. Demidov, V. Lushchikov, S. Nikolaev, Y. Panin, Y. Pokotilovskij, A. Strelkov, and F. Shapiro, [in Russian] Aqueous and zirconium-hydride converters of ultracold neutrons. Neutron confinement in copper and glass vessels., Proc. All-Union conference on neutron physics 4, 264 (1974).
- [41] T. Neulinger, H. Filter, and O. Zimmer, Vertical timeof-flight spectroscopy of ultracold neutrons, Nuclear Instruments and Methods in Physics Research Section A: Accelerators, Spectrometers, Detectors and Associated Equipment 1059, 168947 (2024).
- [42] A. Steyerl, H. Nagel, F.-X. Schreiber, K.-A. Steinhauser, R. Gähler, W. Gläser, P. Ageron, J. Astruc, W. Drexel, G. Gervais, and W. Mampe, A new source of cold and ultracold neutrons. Physics Letters A 116, 347 (1986).
- [43] G. Bison, W. Chen, P.-J. Chiu, M. Daum, C. B. Doorenbos, K. Kirch, V. Kletzl, B. Lauss, D. Pais, I. Rienäcker, et al., Time-of-flight spectroscopy of ultracold neutrons at the PSI UCN source, The European Physical Journal A 59, 215 (2023).
- [44] D.-T. Wong, M. Hassan, J. Burdine, T. Chupp, S. Clayton, C. Cude-Woods, S. Currie, T. Ito, C.-Y. Liu, M. Makela, et al., Characterization of the new ultracold neutron beamline at the LANL UCN facility, Nuclear Instruments and Methods in Physics Research Section A: Accelerators, Spectrometers, Detectors and Associated Equipment 1050, 168105 (2023).
- [45] R. Golub and S. K. Lamoreaux, Neutron electric-dipole moment, ultracold neutrons and polarized ³He, Physics Reports 237, 1 (1994).
- [46] M. Ahmed, R. Alarcon, A. Aleksandrova, S. Baeßler, L. Barron-Palos, L. Bartoszek, D. Beck, M. Behzadipour, I. Berkutov, J. Bessuille, et al. (nEDM), A New Cryogenic Apparatus to Search for the Neutron Electric Dipole Moment, JINST 14 (11), P11017.
- [47] S. Degenkolb, P. Fierlinger, and O. Zimmer, Approaches to high-density storage experiments with in-situ production and detection of ultracold neutrons, Journal of Neutron Research 24, 123 (2022).
- [48] O. Zimmer and R. Golub, Ultracold neutron accumulation in a superfluid-helium converter with magnetic multipole reflector, Phys. Rev. C 92, 015501 (2015).